Assessment of an hybrid process coupling ozonation and anodic oxidation in a monophasic configuration

Helios Yasmine, Florence Fourcade, Fares Zouaoui, Pierre-Francois Biard

Assessment of an hybrid process coupling ozonation and anodic oxidation in a monophasic configuration

Helios YASMINE[a], Florence FOURCADE[a], Fares ZOUAOUI[a], Pierre-François BIARD[a*]

[a]Univ Rennes, Ecole Nationale Supérieure de Chimie de Rennes, CNRS, ISCR – UMR6226, F-35000 Rennes, France

*corresponding author: Pierre-François BIARD, pierre-francois.biard@ensc-rennes.fr

Abstract

This prospective study assessed a hybrid process that combines ozonation with anodic oxidation (AO/O_3) with two boron-doped diamond (BDD) electrodes to treat a model aqueous solution containing 30 ppm of alachlor at pH 5 in a phosphate buffer. An innovative monophasic configuration, operated batch-wise, in which an ozone-stock solution was injected at t_0 in the electrochemical reactor, was proposed in order to avoid introduction of ozone-enriched gas bubbles. The alachlor parent molecule was almost entirely degraded within around 150 min of reaction time by anodic oxidation alone, whatever the applied current intensity (200, 500 and 800 mA). The mineralization efficiency varied from 50% at 200 mA to 80% at 800 mA after 120 min. The results emphasized that the anodic oxidation was a diffusion-controlled process. Addition of ozone at a low ozone dose of 1.9-2.3 mol of ozone per mol of alachlor allowed to decrease the ozone half-life time 2.7 times with the hybrid process compared to ozonation alone. This faster ozone consumption was concomitant with an enhanced alachlor degradation rate, with a corresponding half-life time around two-times lower. However, owing to the low ozone dose applied and the short ozone lifetime in solution (around 25-30 min), similar mineralization efficiencies were noticed for both AO/O_3 and AO processes. Thus, the application of pulse ozone-stock solution re-injections every 20 min to prolong the ozone exposure was assessed to overcome this limitation. However, the effect on the

mineralization rate remained small, even if it allows to enhance even more the alachlor parent molecule degradation rate. The low influence of the hybrid process on the mineralization rate was attributed to the production of aliphatic fatty acids by-products that are poorly reactive with hydroxyl radicals, and whose the degradation by AO is the rate limiting step.

Keywords

Anodic oxidation, ozonation, advanced oxidation process, hydroxyl radicals, alachlor

Highlights

- Assessment of an hybrid ozonation/anodic oxidation monophasic process
- Enhancement of the ozone decomposition rate by the hybrid process
- Enhancement of the alachlor parent molecule degradation rate by the hybrid process
- Low influence of the hybrid process on the mineralization rate
- Pulse reinjections of ozone allows to enhance even more alachlor degradation rate

Graphical abstract

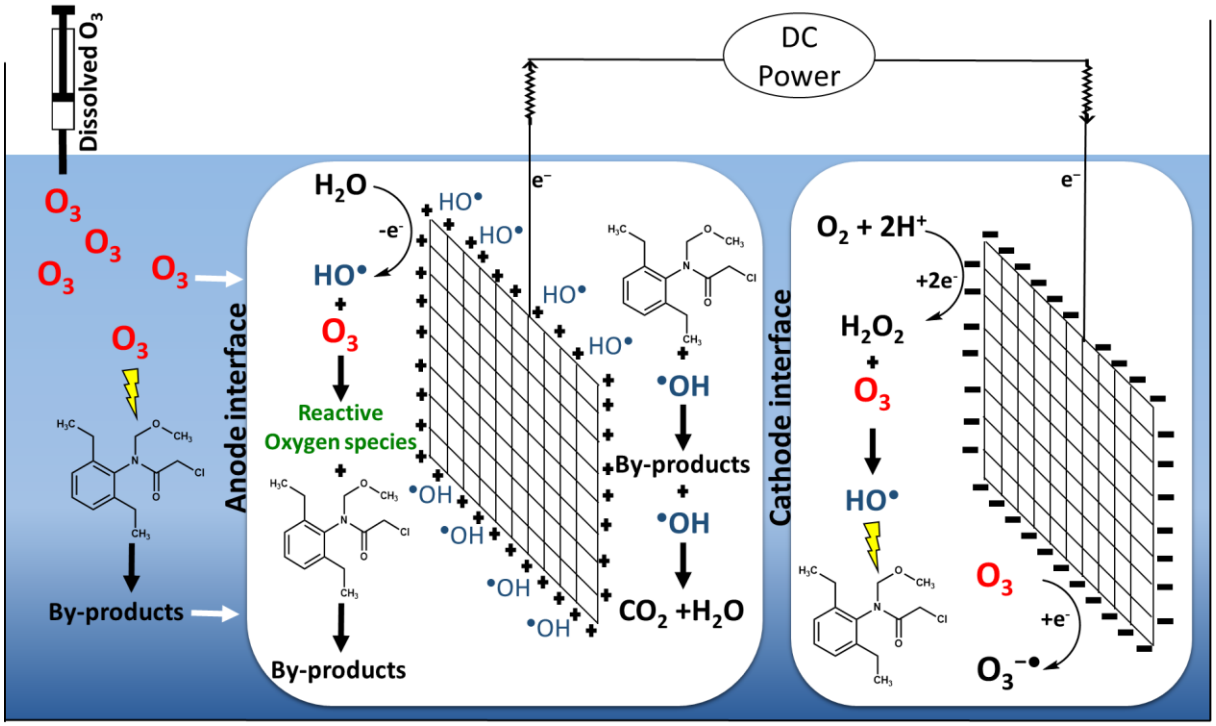

Nomenclature

AO: anodic oxidation

AOP: advanced oxidation process

A_{BDD}: BDD anode surface (33 cm^2)

ARE: average relative error (-)

BDD: boron-doped diamond

C_i: concentration of any species (mol L^{-1} or mol m^{-3})

COD: chemical oxygen demand (mol_{O_2} L^{-1})

CE: current efficiency (-)

D_i: diffusion coefficient of any species i (m^2 s^{-1})

DET: direct electron transfer

DOC: dissolved organic carbon (ppm)

Eff: removal efficiency (-)

EfOM: effluent organic matter

$f_{HO^\bullet}$: fraction of hydroxyl radicals reacting with alachlor (-)

H: ozone Henry's law constant (Pa m^3 mol^{-1})

I: current intensity (A)

J: current density (A m^{-2} or mA cm^{-2})

k: reaction rate constant (mol^{1-n} L^{n-1} s^{-1})

k_m and k_L: mass-transfer coefficient in the liquid phase for COD and O_3, respectively (m s^{-1})

n: order of reaction (-)

OM: organic matter

R_{ct}: ratio of the hydroxyl radical exposure to the ozone exposure (-)

ROS: reactive oxygen species

S: gas-liquid interfacial area (m^2)

$t_{1/2}$ and $t_{0.2}$: half-life time and time for a removal efficiency of 20%, respectively (min or s)

TOC: total organic carbon (ppm)

V: volume (L or m^3)

Subscripts:

al: alachlor

app: apparent

H_2O_2: hydrogen peroxide

G: in the gas-phase

i: any species i

L: in the liquid-phase

oz: ozone

0: at t_0

1. Introduction

Industrial wastewaters treatment needs nowadays technologies, such as ozone-based or electrochemical advanced oxidation processes (AOPs), able to reach extensive mineralization of the organic pollutants. Table S.1 presents the main mature or in development processes to remove organic pollutants from wastewaters. One strategy to improve refractory compounds removal is to combine these processes under a multi-barrier approach.

Ozonation is widely used in drinking water production plant and is more and more considered for industrial and urban waste waters treatment, owing to its reactivity on organic matter and emerging pollutants [1–5]. Its reactivity in aqueous solution relies on two pathways, the direct pathway which involves molecular ozone, and the indirect pathway which involves reactive oxygen species (ROS), especially hydroxyl radicals $HO^{\bullet}$, generated from the spontaneous ozone decomposition in water [4,6,7]. In natural waters (ground water, surface water, etc.) and waste waters, the ozone decomposition is mainly initiated through the reaction with the hydroxide anion and with some electron-rich moieties of the organic matters, particularly when they have deprotonated functions (such as carboxylates, phenolates, etc.), that electrophilic molecular ozone can easily target [5,8,9]. Consequently, the ozone decomposition reaction rate typically increases with the pH. To enhance both the ozone decomposition and ROS generation rates, chemical (catalyst, H_2O_2) or physical (UV, US) initiators can be also added in ozone-based AOPs [7].

More recently, several authors investigated the potential of hybrid ozone/electrochemical processes. Electrochemical processes are recognized as versatile, easily automable and are operated in mild conditions [10–14]. There are several ways to combine ozonation and electrochemical processes [10,15–20]. Among them, the most studied are i) the electrochemical production of ozone [16,21,22], ii) the electroperoxone process [23–28] and iii) the combination between anodic oxidation and ozonation.

The electroperoxone process is based on the coupling of ozone and *in-situ* produced hydrogen peroxide from the electrochemical reduction of oxygen [14,29,30]. Both the electrochemical reduction of O_3 and the reaction between O_3 and the hydroperoxyde anion (the conjugated base of H_2O_2) generate ROS. Carbon based materials and gas diffusion electrodes are preferentially chosen as cathode materials in this combined process owing to the fact that they favour the H_2O_2 production [14,24,31].

Anodic oxidation (AO) has emerged as an efficient, easy, environmentally friendly and cost-effective treatment process for removing persistent organic compounds [32–34]. AO can degrade and mineralize pollutants through both direct and indirect processes. Indeed, on the electrode surface,

organic pollutants can be directly oxidized or reduced through the exchange of electrons with the electrode surface. This mechanism is called direct electron transfer (DET). Besides, pollutants can also be oxidized by an indirect oxidation process through the *in-situ* generation of various oxidants, particularly $HO^{\bullet}$ radicals produced at the anode surface through the oxidation of H_2O [35,36]. The efficiency of the AO process and the nature and amount of reactive species formed can be affected by various factors, including the material of the electrode, the type of contaminant, the type of electrolyte and the applied current or voltage [37].

The limitations of each processes can be surpassed by the combination of the two processes. On one hand, O_3 degradation preferably leads to short chain aldehydes and carboxylic acids, non-reactive with O_3 and poorly reactive with hydroxyl radicals, limiting the mineralization of the pollution [5,38]. Electrochemical processes are more potent to mineralize organic compounds than ozonation owing to the DET mechanism that can potentially target organic compounds refractory to reactions with hydroxyl radicals, such as low-chain fatty acids. Furthermore, electrochemical processes might be able to efficiently decompose O_3 even at acidic pH, due to ozone reactions at both the cathode and anode's surface, allowing to increase the pH window of ozone reactivity. On the other hand, the formation of polymer by the electrochemical oxidation of cyclic compounds entails electrode fouling and decreases the current efficiency (CE) [39]. Ozone can react with phenolic compounds by ring opening (cycloaddition mechanism) leading to a reduction of the polymer formation. Biofilm formation at the electrodes surface would be also potentially mitigated by the use of ozone.

Thus, the removal of various persistent organic pollutants by hybrid anodic oxidation/ozonation (OA/O_3) processes was studied in aqueous solution [20,23,40,41] and in sludge from wastewater treatment plant [42]. Compared to sole electrooxidation, higher and faster removal yields were obtained highlighting the synergy between ozonation and electrooxidation [19,23,40].

The most studied anode material is the boron-doped diamond (BDD) characterized by a good chemical stability and an important production of physisorbed hydroxyl radical [10,20,23,42–44]. Ti/PbO_2 anodes are also pertinent candidates because, as for the BDD, the overpotential for O_2 evolution is high [40]. The applied current densities were at the same order of magnitude as for the electroperoxone process, from around 10 to 60 mA cm^{-2} [20,23,40–42]. Only a few papers investigated the influence of the pH even if it strongly influences the O_3 decomposition [20,40]. Qiu *et al.* assessed the influence of the nature and the concentration of the supporting electrolyte [45]. In Na_2SO_4 electrolyte, the mineralization increased with the concentration and the formation of sulfate radicals was supposed. In NaCl electrolyte, the formation of active chlorine species improved the combined process efficiency but the formation of refractory chlorinated intermediates was suspected. An increase of the current density enhanced the production of hydroxyl radicals at the

anode. They also concluded that, in their study, the O_3 reduction at the cathode played only a minor role on the p-nitrophenol degradation [45].

In the majority of the hybrid OA/O_3 process studies, ozone-enriched gas bubbles were used to feed the electrochemical reactor. In that case, the ozone transfer in solution and the oxidation processes were achieved in only one stage. However, particularly in waste waters, which are characterized by a high effluent organic matter (EfOM) content and consequently by a high ozone demand [46], the ozone reaction rate in the boundary layer can be higher than the ozone transfer rate (fast kinetic regime) [7]. Thus, ozone would be completely consumed at the vicinity of the gas-liquid interface and wouldn't be able to reach the surfaces of the anode and cathode. Nonetheless, for other kinds of hybrid ozonation processes, the relevance of mixing a pre-ozonated solution to the water to treat, instead of using ozone-enriched gas bubbles, has been demonstrated [47,48]. It requires to dissociate the ozone transfer step and the oxidation steps. This approach is beneficial to locate the ozone decomposition, and the ROS generation in the liquid bulk, not at the gas-liquid interface. Furthermore, it enables to advantageously control the ozone dose introduced.

Consequently, the purpose of the present prospective study is to investigate the potential of a hybrid process coupling ozonation and anodic oxidation in a batch monophasic system, in which a known volume of an ozone stock solution was added to the studied water matrix. BDD anodes and cathodes were used owing to their high potential of $HO^{\bullet}$ generation. An acidic pH of 5 was selected in order to limit the ozone decomposition initiated by the hydroxide anions in the bulk and to assess more particularly the mechanisms involved between dissolved ozone and both BDD electrodes. A phosphate buffer as supporting electrolyte was preferred to conventional Na_2SO_4 and NaCl electrolytes, allowing to avoid the formation of chlorine and sulfate radical reactive species, in order to focus only on the mechanisms associated to ROS generation and DET.

2. Material and methods

2.1. Experimental set-up description

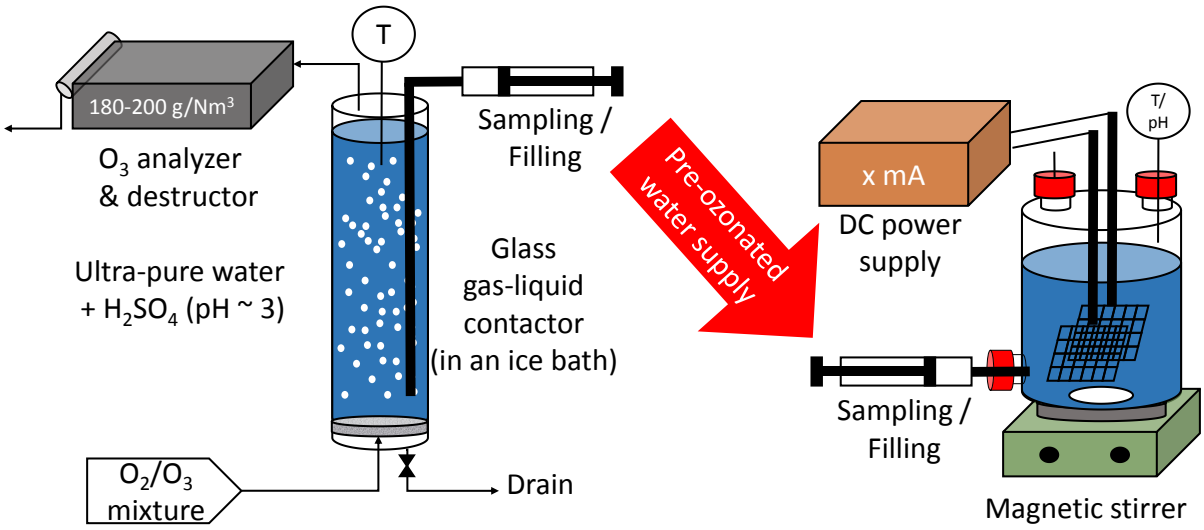

Figure 1: Scheme of the experimental procedure.

A module, already described elsewhere [49], allowed to produce an ozone-enriched oxygen flow (at a concentration in the range 180-200 g Nm^{-3} and a flow rate of 15 NL h^{-1}, under the normal conditions for temperature and pressure). The ozone/oxygen mixture was continuously bubbled in a custom glass bubble column equipped with a gas sparger at the bottom. The bubble column was placed in an ice bath to set a temperature around 1°C. The bubble column contained 1 L of ultra-pure water (UPW) acidified at pH 2 through the addition of 3.75 mL of H_2SO_4 at 1 M, in order to completely suppress ozone decomposition. After ~ 30 min, the gas-liquid equilibrium was reached within the bubble column at a dissolved ozone concentration around 100 ppm.

In parallel, 700 mL of the studied aqueous solution (ultra-pure water doped with alachlor and a phosphate buffer to set a pH ~ 5) was introduced in a custom magnetically stirred glass reactor containing 2 BDD grid electrodes (50×50×1.4 mm corresponding to a surface of 33 cm^2) connected to a DC power supply unit (Microlab, provided by Micronics-System) by Platinum wires. The electrodes, provided by NeoCoat SA (Switzerland), were composed of 6 µm Boron-Doped Diamond deposited on a niobium substrate (Nb doped with 2500 ppm of boron). The interlectrode distance

was set at 1.5 cm. Three current intensity were assessed, 200, 500 and 800 mA, corresponding to current densities J of 6.1, 15.2 and 24.2 mA cm^{-2}, respectively. A sampling port equipped with a Luer-Lock valve, located at the bottom of the electrochemical reactor, allowed to introduce and withdrawn samples with a set of different gas-tight syringes (provided by Hamilton or SGE).

At t_0, 100 mL of the ozone-stock solution (or of UPW when only anodic oxidation was evaluated) was added as fast as possible (~ 10 s) in the electrochemical reactor to the 700 mL alachlor solution using a 100 mL gas-tight syringe (Hamilton). Thus, it lead to a total liquid volume (V_L) of 800 mL and an initial alachlor concentration around 30 ppm (corresponding to a DOC concentration of ~ 19 ppm), a phosphate buffer concentration of 50 mM and a conductivity of 4.52 mS cm^{-1} at 20°C. The initial ozone concentration was typically in the range from 10 to 13 ppm. Regular samples were withdrawn but the total amount of solution removed was kept lower than 10% of the initial volume. An excess of sodium bisulfite in powder was used to quench ozone residuals in the vials in which samples for alachlor and TOC quantification were collected.

To avoid pressure variations during filling and withdrawing, a metal hub needle was introduced in the top of the reactor, allowing to keep the atmospheric pressure inside the electrochemical reactor but with very limited gas transfer between the gas headspace and the atmosphere outside the reactor. The ozone desorption from the aqueous phase to the gas headspace was previously assessed by measuring the dissolved ozone concentration with an unreactive aqueous solution. The ozone desorption percentage did not exceed 20% in 40 min (See part 3.1.1) and was even lower in reactive systems, prone to consume ozone in lower time ranges.

2.2. Analytical methods

Alachlor quantification was achieved with a Waters Acquity UPLC H-Class Plus chromatographic chain equipped with a Waters PDA eλ (Photodiode Array Detector) and a Waters quaternary solvent manager. The separation was performed on a column Acquity UPLC BEH C-18 (1.7 µm; 2.1 × 100 mm)

208 at 45°C with a gradient elution process based on two solvents (A: UPW / Acetonitrile + 0.1% formic
209 acid 10/90 and B: Acetonitrile + 0.1% formic acid). Samples were analyzed after filtering through a
210 0.2 μm membrane filter. The ozone concentration was selectively quantified by the Indigo method
211 [50]. A Helios UV–Vis spectrophotometer (Shimadzu, Japan) was used for the indigo absorbance
212 measurement, performed a few minutes after the sampling (λ = 600 nm). The H_2O_2 concentration
213 was determined through the potentiometric titration of I_2, generated by the oxidation of KI by H_2O_2,
214 employing sodium thiosulfate as the titrant. Total Organic Carbon was quantified by a Shimadzu COT-
215 meter (TOC-V CPH) with the NPOC method.

3. Results and discussion

3.1 Direct oxidation study by cyclic voltammetry

Cyclic voltamogramms were recorded to examine the electrochemical behavior of alachlor on the BDD electrodes at a scan rate of 100 mV s^{-1} in a 50 mM H_3PO_4 aqueous solution. Current-potential curves were plotted in the absence and in the presence of 30 ppm of alachlor (Fig. 2). The oxygen evolution potential was observed at around 1.8 V vs. SCE and the hydrogen evolution reaction was observed at around -0.8 V vs. SCE. Oxygen reduction was observed around -0.1 V vs. SCE but no signal appeared for alachlor on the BDD electrode in the electroactivity range of the supporting electrolyte. It shows that direct electron transfer does not occur between BDD electrode surface and alachlor molecule before both oxygen evolution and hydrogen evolution reactions. However, the direct oxidation or reduction of alachlor remains possible at potentials outside the electroactivity range of the BDD electrodes. For instance, He et *al.* demonstrated that alachlor could be reduced on a glassy carbon electrode at -1.25 V vs. SCE [51].

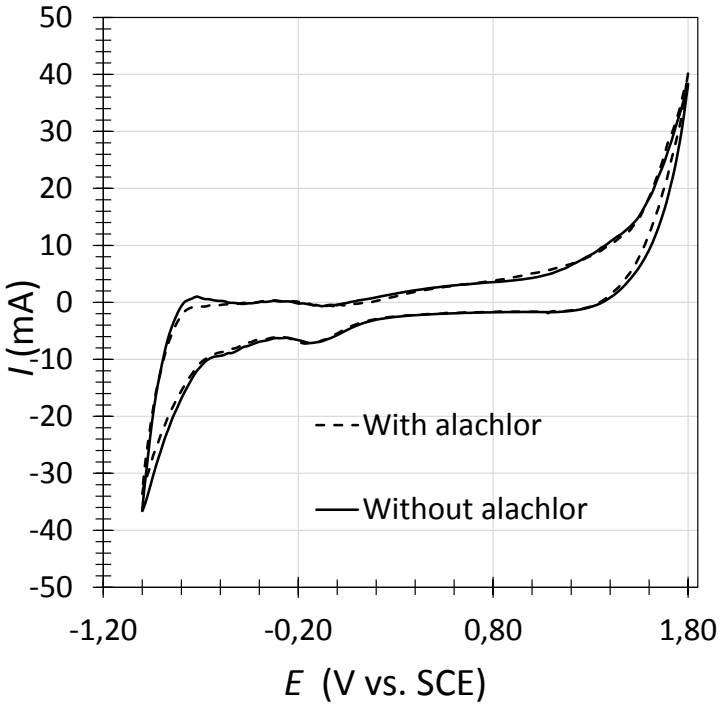

Figure 2. Cyclic voltammograms in 50 mM H_3PO_4 with and without 30 ppm alachlor using BDD electrodes.

3.2 H_2O_2 electrochemical generation

The combined use of ozone/hydrogen peroxide (O_3/H_2O_2) accelerates the conversion of O_3 to $HO^{\bullet}$, which can reduce the reaction time required for pollutants degradation [52]. Therefore, there has been an increased interest in inducing the *in-situ* production of H_2O_2 to enhance O_3 decomposition efficiency. Anodic oxidation generally induces the production of H_2O_2 at the cathode. In the light of this, the production of H_2O_2 in function of the electrolysis duration and the current density (50, 100 and 500 mA) is presented in Fig. 3. H_2O_2 generation began as soon as the electrodes were polarized and continued to increase up to 80 minutes regardless of the applied current intensity. After 80 minutes, the concentration of H_2O_2 remains almost constant, indicating the establishment of an equilibrium between the cathodic production of H_2O_2 and its anodic oxidation. For low current intensities, the production of H_2O_2 increased with the applied current intensity. However, for 500 mA, the production of H_2O_2 is lower than for 50 and 100 mA. This behavior can be explained owing to the fact that for high current intensities, hydrogen evolution and 4 electrons reduction of O_2 into H_2O compete with H_2O_2 formation. According to the state of the art, a similar behavior has been observed with a graphite cathode [53].

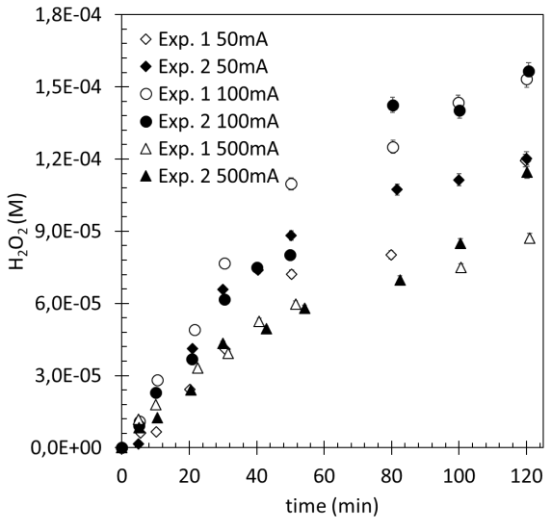

Figure 3. H_2O_2 concentration evolution in function of the electrolysis duration for different current intensities (50, 100 and 500 mA) using BDD electrodes in 800 mL H_3PO_4 at 60 mM.

3.3. Ozonation alone

3.3.1 Ozone desorption in the electrochemical reactor

The ozone desorption from the liquid phase to the gas headspace in the electrochemical reactor was firstly evaluated (See Part S.2). The electrochemical reactor was filled with an ultra-pure water acidified at pH 3.5 through 0.1 M H_2SO_4 addition and containing tBuOH (0.005 M) as radical scavenger in order to prevent ozone decomposition [4]. Experiments were performed with or without the non-polarized BDD electrodes. Around 20% of the ozone dose introduced at t_0 was desorbed after 40 min (Fig. S.2) and no significant difference was observed with or without electrodes, showing that no ozone decomposition occurred at the uncharged electrode surface. The time profile of the ozone concentration was modeled according to Eq. S.8 which allowed to determine by numerical resolution the average value of the ozone liquid-side mass-transfer coefficient k_L (k_L = 1.94×10^{-5} m s^{-1}) at T = 19 ± 1°C. This value is in good agreement with the value of 1.19×10^{-5} m s^{-1} found for ozone in a stirred-cell reactor agitated by a Rushton turbine at 20°C [49].

3.3.2 kinetic modeling

Taking into account the ozone desorption from the liquid phase to the gas headspace (part 3.3.1 and part S.2) and the ozone decomposition in the electrochemical reactor, Eq. 1 is obtained:

$$-\frac{dC_{L,oz}}{dt} = \frac{k_L S}{V_L}\left(C_{L,oz} - \frac{RT}{H}C_{G,oz}\right) + k_{app}{C_{L,oz}}^{n} \quad \text{(Eq. 1)}$$

With k_{app} (mol^{1-n} L^{n-1} s^{-1}) the apparent ozone decomposition reaction rate constant and n the order of reaction. S is the surface area between the liquid-phase and the gas-phase, corresponding to the electrochemical reactor section (7.76×10^{-3} m^2). V_L is the liquid volume (m^3). H (Pa m^3 mol^{-1}) is the ozone Henry's law constant in water deduced from the correlation of Ferre-Aracil et al. [54]. The

ozone gas-phase concentration $C_{G,oz}$ is related to the ozone liquid-phase concentration $C_{L,oz}$ through Eq. 2:

$$\frac{k_L S}{V_L}\left(C_{L,oz} - \frac{RT}{H} C_{G,oz}\right) = \frac{dC_{G,oz}}{dt} V_G \qquad \text{(Eq. 2)}$$

The best values of n and k_{app} associated to each experiment were determined by numerical resolution following the procedure presented in supplementary material (Part S.3). The knowledge of these parameters allowed for each experiments to model $C_{L,oz}$ vs time and to determine both the ozone half-life time ($t_{1/2}$) according to Eq. 3 and the ozone exposure ($\int C_{L,oz} dt$) according to Eq. 4 [55]:

$$t_{1/2} = {C_{L,oz,0}}^{1-n} \frac{\left(2^{n-1}-1\right)}{k_{app}(n-1)} \text{ if } n \neq 1 \text{ and } t_{1/2} = \frac{\ln(2)}{k_{app}} \text{ if } n = 1 \qquad \text{(Eq. 3)}$$

$$\int_{t_0}^{t} C_{L,oz} dt = \sum_{i=1}^{m} \frac{C_{L,oz,i-1} + C_{L,oz,i}}{2} \times \Delta t \qquad \text{(Eq. 4)}$$

With m the number of time-interval Δt (fixed to 12 s).

The alachlor degradation rate can be modeled according to Eq. 5 considering bimolecular reactions with both $HO^{\bullet}$ and O_3 [56]:

$$-\frac{dC_{al}}{dt} = k_{O_3} C_{L,oz} C_{al} + k_{HO^{\bullet}} \cdot C_{HO^{\bullet}} \cdot C_{al} \quad \text{(Eq. 5)}$$

With k_{O_3} the reaction rate constant between O_3 and alachlor and $k_{HO^{\bullet}}$ the reaction rate constant between $HO^{\bullet}$ and alachlor, presumed equal at 2.8 ± 0.3 L mol^{-1} s^{-1} and 3.2×10^{10} L mol^{-1} s^{-1}, respectively, according to Beltran et al. [56]. Thus, Eq. 5 can be rearranged leading to Eq. 6:

$$\ln\left(\frac{C_{al}}{C_{al,0}}\right) = k_{O_3} \int_{t_0}^{t} C_{L,oz} dt + k_{HO^{\bullet}} \int_{t_0}^{t} C_{HO^{\bullet}} dt \qquad \text{(Eq. 6)}$$

The $HO^{\bullet}$ generation can be quantified in ozonation processes with the R_{ct} concept, which corresponds to the ratio of the $HO^{\bullet}$ exposure ($\int C_{HO^{\bullet}} dt$) to the ozone exposure ($\int C_{L,oz} dt$). Thus, Eq. 6 leads to Eq. 7:

$$\ln\left(\frac{C_{al}}{C_{al,0}}\right) = \left(k_{O_3} + k_{HO^\bullet}R_{ct}\right)\int_{t_0}^{t} C_{L,oz}dt <=> C_{al} = C_{al,0}\exp\left(\left(k_{O_3} + k_{HO^\bullet}R_{ct}\right)\int_{t_0}^{t} C_{L,oz}dt\right) \quad \text{(Eq. 7)}$$

The R_{ct} is usually constant after the instantaneous ozone demand phase in natural and synthetic waters [57]. It was determined by numerical resolution for each experiment by trying to minimize the sum of square errors (SSE) between the experimental and modeled values of C_{al}. The knowledge of the R_{ct} value allowed to determine the fraction of alachlor reacting with $HO^\bullet$ ($f_{HO^\bullet}$) according to Eq. 8 [57]:

$$f_{HO^\bullet} = \frac{k_{HO^\bullet}R_{ct}}{k_{HO^\bullet}R_{ct}+k_{O_3}} \quad \text{(Eq. 8)}$$

In the present study, in which the water matrix was deprived of natural organic matters, the instantaneous ozone demand was systematically negligible.

3.3.3 Alachlor degradation by ozonation

Alachlor oxidation by only ozone was assessed in the electrochemical reactor with the non-polarized BDD electrodes at low ozone doses in the range 0.4-0.6 g_{O_3} g_{DOC}^{-1} (~ 2-2.5 mol_{O_3} mol_{al}^{-1}). The time-course profiles of both the ozone and alachlor concentrations are provided in Fig. 4. No mineralization was observed (Fig. S.4) with a constant DOC concentration over time, which is consistent with the low ozone doses applied.

Without radical scavenger (tBuOH) added, the ozone half-life time (Eq. 3), was around 12 min (Table 1). Owing to the low applied ozone dose, the alachlor degradation was not complete and reach a maximal removal efficiency of around 50-60% after ~ 35 min and the full O_3 decomposition (Fig. 4.a). The ozone decomposition was well described by a 0.8^{th}-order rate law (Table 1). The ozone decomposition rate observed was four orders of magnitude higher than the one corresponding to the initiation reaction of molecular ozone with the hydroxide anion at the low pH applied (*i.e.* $k_{O_3/HO^-}C_{HO^-}C_{L,oz} << k_{app}C_{L,oz}^{0.8}$) [8]. It shows that the ozone decomposition was initiated by another reactions,

which involve directly the alachlor parent molecule and/or some of its intermediates. The R_{ct} value of 0.76×10^{-10}, is two to three orders of magnitude lower than in natural and waste waters [5,57], which emphasizes a low potential of $HO^{\bullet}$ generation in the investigated water matrix which is deprived of natural and effluent organic matters acting as potent ozone decomposition initiators. Thus, a fraction of alachlor reacting with $HO^{\bullet}$ ($f_{HO}\bullet$) of 63% was determined (Eq. 8), showing that both the direct (involving molecular ozone) and indirect (involving free hydroxyl radicals) pathways were concomitant. In natural and waste waters in which organic matters would be present, higher R_{ct} would be expected and a complete oxidation by $HO^{\bullet}$ would be observed [1].

With the addition of tBuOH as radical scavenger, both the ozone decomposition and alachlor degradation rates were significantly slowed down compared to the experiments without tBuOH (Fig. 4). The ozone half-life time (42 min) was around 3.5 times higher than without radical scavenger (Table 1). More precisely, the alachlor removal efficiency was also a little bit lower, around 43% after 40 min but the ozone consumption was not complete yet. Furthermore, the R_{ct} was negligible demonstrating that the tBuOH concentration of 0.01 M was sufficient to efficiently scavenge all the radicals formed by the ozone decomposition in presence of alachlor. The ozone decomposition kinetics was well described by a first-order rate law accounting for molecular O_3 reaction with the alachlor parent molecule and also with some degradation intermediates because the apparent stoichiometry of the reaction was not constant over time and varied between 3 mol and 4.5 mol of O_3 consumed per mol of alachlor consumed. The alachlor concentration-time profile was modeled by Eq. 7, and the alachlor consumption was too sharp using the value of k_{O_3} proposed by Beltran et al. [56], with an average relative error (*ARE*) of 26% between the experimental and modeled values of C_{al}. Thus, the value of k_{O_3} was recalculated by numerical resolution using Eq. 7 and an alternative lower value of 1.39 L mol^{-1} s^{-1} was determined, associated to an *ARE* for C_{al} of only 1.9%.

Furthermore, a reference experiment with an initial concentration 100 µM of H_2O_2 allowed to simulate the potential influence of the H_2O_2 electrogeneration (See Part 3.2). An enhancement of the

ozone decomposition reaction rate, with an ozone half-life time of only 6 min, was observed (Table 1 and Fig. 4.a). The ozone decomposition rate linked to the ozone decomposition by the hydroperoxyde anion can be estimated through the calculation of the product of the reaction rate constant k_{O_3/HO_2^-} with the HO_2^- concentration $\left(k_{O_3/HO_2^-} \times C_{HO_2^-}\right)$, taking into account a maximal total H_2O_2 concentration ($C_{H_2O_2}$) of 100 μM and a *pKa* (H_2O_2/HO_2^-) of 11.75 according to Eq. 9 [58]:

$$k_{O_3/HO_2^-} C_{HO_2^-} = k_{O_3/HO_2^-} \frac{C_{H_2O_2}}{1+10^{pKa-pH}} = 2.40 \times 10^6 \frac{100\times10^{-6}}{1+10^{11.75-5}} = 4.3 \times 10^{-5}\ s^{-1} \quad \text{(Eq. 9)}$$

Thus, the ozone decomposition rate linked to the ozone decomposition by the hydroperoxyde $\left(k_{O_3/HO_2^-} C_{HO_2^-} C_{L,oz}\right)$ is around 50 times lower than the apparent ozone decomposition rate ($k_{app} C_{L,oz}^{0.8}$) considering an average ozone concentration of 100 μM. It shows that the potential H_2O_2 electrogeneration would contribute poorly directly to the ozone decomposition initiation in the liquid bulk owing to the low pH applied. Nonetheless, the presence of a moderate H_2O_2 concentration can promote the ozone decomposition owing to the fact that H_2O_2 can react with $HO^\bullet$ leading to the hydroperoxyl radical $HO_2^\bullet$, which is in equilibrium with the superoxide radical $O_2^{\bullet-}$ that reacts further with O_3 leading to the ozonide radical $O_3^{\bullet-}$ ensuing the radical chain [59–62]. Thus, the R_{ct} value was around twice with H_2O_2 (Table 1). Yong and Lin demonstrated that the R_{ct} corresponds to the ratio of the total initiation capacity to the total inhibition capacity of a water matrix [63]. Considering that the inhibition capacity should not depend on the addition of H_2O_2, it shows that the initiation capacity is doubled. Consequently, the initiation reaction with the hydroperoxyde anions contributes almost equally with the other initiation reactions. It also confirms that promotion reactions with some oxidation intermediates contribute importantly to the ozone decomposition rate, even if they do not influence the R_{ct} [63]. Nonetheless, with H_2O_2, associated to a lower ozone exposure because of the faster ozone decomposition, the final hydroxyl radical exposure ($\int_{t_0}^{t} C_{HO^\bullet} dt$) and ensuing alachlor final removal efficiencies were similar with/without H_2O_2 (Table 1). It confirms that addition of H_2O_2 does not necessarily leads to better removal efficiencies but advantageously allow to speed

363 up the oxidation process. Finally, evaluation of the fraction of alachlor reacting with $HO^{\bullet}$ ($f_{HO\bullet}$) is

364 promoted using H_2O_2 and shift from 63% to 81% (Table 1).

365

Table 1. Values of the apparent reaction rate constants accounting for the ozone decomposition (k_{app}), ozone half-life time, alachlor removal efficiency EFF_{al} after 40 min, R_{ct}, $HO^{\bullet}$ exposure and $f_{HO}^{\bullet}$ by only ozonation (non-polarized BDD electrodes, pH 5, V_L = 800 mL, $C_{al,0}$ ~ 108 μM, $C_{L,oz,0}$ ~ 200-280 μM).

	With tBuOH (0.1 M)	Without tBuOH	With H_2O_2 (100 μM)
n	1	0.8	0.8
k_{app} ($mol^{1-n}\ L^{n-1}\ s^{-1}$)	1.81×10^{-4}	2.77×10^{-4}	3.48×10^{-4}
$t_{1/2}$ O_3 (min)	42	12	6
ARE (C_{O_3})	4%	9%	16%
Eff_{al} at 40 min	43%	50-60%	48%
ARE (C_{al})	1.9%	1.9%	1.2
$10^{10}\times R_{ct}$	Negligible	0.76	1.89
$f_{HO}^{\bullet}$		63%	81%
$10^{11}\times\int_{t_0}^{t} C_{HO}\cdot dt$ (M s)		1.6	1.7

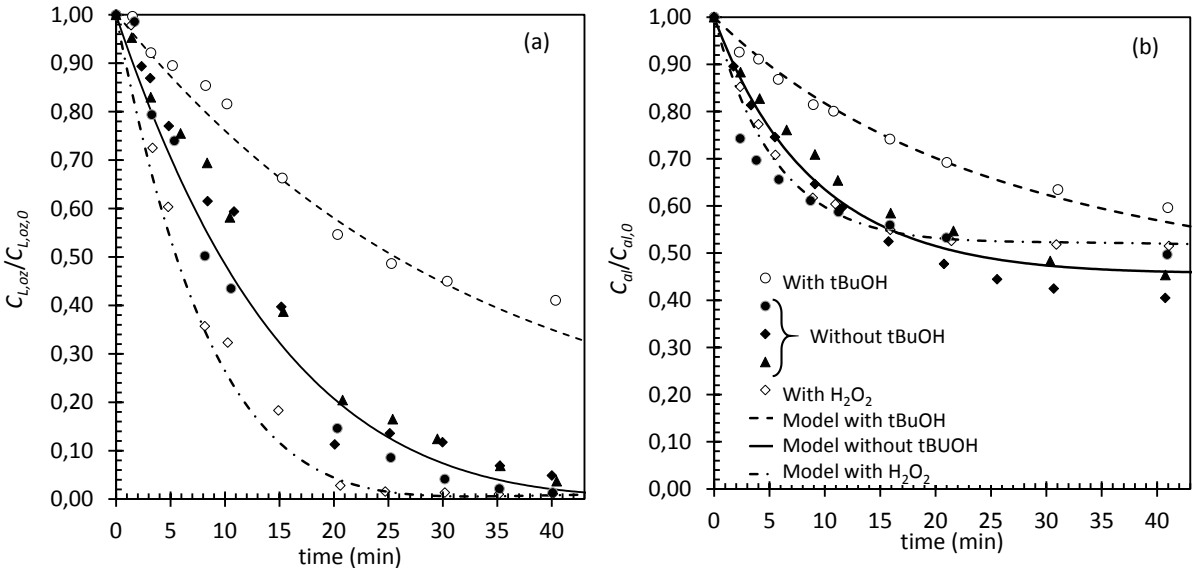

Fig. 4. Time-course profile of $C_{L,oz}/C_{L,oz,0}$ (a) and $C_{al}/C_{al,0}$ (b) by only ozonation (non-polarized BDD electrodes, pH 5, V_L = 800 mL, $C_{al,0}$ ~ 108 μM, $C_{L,oz,0}$ ~ 180-280 μM). Dark symbols: triplicate experiments without H_2O_2 and without tBuOH. Empty circles: reference experiment with tBuOH (0.01 M). Empty diamond: reference experiment with H_2O_2 (100 μM at t_0). Lines correspond to the model (Eqs. 1,2 and 7).

3.4. Anodic oxidation

3.4.1 Alachlor anodic oxidation

Contrarily to single ozonation, anodic oxidation enabled to fully degrade alachlor but with a reaction time around 150 min (Fig. 5.a). Surprisingly, the alachlor reaction rate did not depend significantly on the applied current intensity. Anodic oxidation allowed to partly mineralize the alachlor parent molecule, with DOC removal efficiencies in the range 50-80% after 120 min of reaction time (Fig. 5.b). In that case, the mineralization rate advantageously increased with the applied current intensity. The alachlor and DOC degradation kinetics were both successfully modeled by a first-order rate law:

$$-\frac{dC_i}{dt} = k_{app,i}C_i <=> C_i = C_{i,0}e^{-k_{app,i}t} \quad \text{(Eq. 10)}$$

The corresponding apparent reaction rate constant ($k_{app,al}$ and $k_{app,DOC}$ in s^{-1}) and half-life times ($\ln(2)/k_{app,i}$) are summarized Table 2. As expected from Fig. 5.a, the alachlor half-life times are erratic and in the range 23-30 min. However, the DOC half-life time significantly droped with the current intensity, shifting from 120 min at 200 mA to 54 min at 800 mA.

The fact that the DOC degradation followed a first-order rate law demonstrates that the electrochemical reactions are diffusion controlled, meaning that alachlor and its intermediates mass-transport to the anode was the rate limiting step and that the imposed current densities are always higher than the limiting current density J_{lim} (A m^{-2}) [64]. Thus, the apparent reaction rate constant was correlated to the DOC mass-transfer coefficient (k_m in m s^{-1}) according to Eq. 11 [64]:

$$k_{app} = \frac{A_{BDD}k_m}{V_L} \quad \text{(Eq. 11)}$$

With A_{BDD} the anode surface (m^2). The mass-transfer coefficients calculated have an order of magnitude of 10^{-5} m s^{-1} (Table 2). k_m increased linearly with the current intensity (inset Fig. 5.b), a behavior which has been already observed in the literature [65]. The y-intercept of k_m vs. the current

intensity provided the limiting value of k_m ($k_{m,lim}$ = 1.35×10^{-5} m s^{-1}) in solution when the difference in potential between the electrodes is null. $k_{m,lim}$ is only slightly lower than the value of k_L of 1.94×10^{-5} m s^{-1} found for O_3 (Part 3.3.1). According to the Danckwerts theory, the ratio of the mass-transfer coefficients is proportional to the square root of the ratio of the corresponding diffusion coefficients according to Eq. 12 [7]:

$$\frac{k_{m,lim}}{k_{m,oz}} = \sqrt{\frac{D_{oz}}{D_{DOC}}} \quad \text{(Eq. 12)}$$

Considering D_{oz} = 1.7×10^{-9} m^2 s^{-1} at T = 20 °C [66], an estimation of D_{DOC} of 0.82×10^{-9} m^2 s^{-1} can be determined, which is consistent with the range of 0.9 - 1.1×10^{-9} m^2 s^{-1} expected for low-chain fatty acids according to the Wilke-Chang correlation at 20°C [67]. Indeed, Qiang et al. demonstrated that the main by-products of alachlor oxidation are small aliphatic organic acids such as formic, acetic, oxalic and propionic acids [68]. These by-products are quite refractory to the hydroxyl radicals attack, with reaction rate constants in the range 10^6 - 8×10^8 L mol^{-1} s^{-1} [69], and can be quickly accumulated in solution [3,34].

The knowledge of k_m enabled to determine the limit current density at t_0 ($J_{lim,0}$) over which the process is diffusion controlled [64]:

$$J_{lim,0} = 4Fk_m COD_0 \quad \text{(Eq. 13)}$$

F is the Faraday's constant. COD_0 is the chemical oxygen demand at t_0 (2.04 $mmol_{O_2}$ L^{-1}), calculated from the initial alachlor concentration and considering that alachlor total mineralization consumes 19 equivalent of O_2 according to the following balanced chemical equation:

$$C_{14}H_{20}ClNO_2 + 19\ O_2 \rightarrow 14\ CO_2 + 2H^+ + NO_3^- + Cl^- + 9\ H_2O \quad \text{(Eq. 14)}$$

The ratio $J_{applied}/J_{lim,0}$ was always higher than 1 (Table 2) confirming that the electrochemical process is diffusion controlled. Finally, the current efficiency (*CE*) was determined by Eq. 15 [64]:

$$CE = \frac{4FV_L}{It}(COD_0 - COD_t) \qquad \text{(Eq. 15)}$$

With *I* the current intensity (A). CE slightly decreased with the reaction time *t* and was maximal at the lower applied current intensity of 200 mA, which highlights a better tradeoff between the energy consumption and the alachlor mineralization at this intensity (Fig. 6). Indeed, at such a lower intensity, parasite reactions corresponding to both O_2 and N_2 degassing are less significant.

Finally, addition of 0.01 M and 0.1 M of tBuOH and 0.01 M ethanol as radical scavengers enables to slightly slow down the alachlor degradation rate (Fig. 5.a). EtOH and tBuOH are both recognized for their ability to scavenge free $HO^{\bullet}$ [70,71]. Thus, it confirms that free $HO^{\bullet}$ are produced during anodic oxidation. However, several authors claims that tBuOH should be also able to scavenge surface bounded $HO^{\bullet}$ [70]. Nonetheless, according to Barazesh et al. [72], saturated alcohols such as tBuOH do not react readily with electrode surfaces. Furthermore, Babu et al. showed that tBuOH can be oxidized through DET using BDD anodes which can affect the conclusions of some authors that used tBUOH to scavenge surface bounded $HO^{\bullet}$ [71]. Consequently, it remains difficult to conclude about the main mechanism of alachlor oxidation involved, which can happen through reactions with surface $HO^{\bullet}$ that tBuOH cannot efficiently scavenge and/or by DET at potentials outside the electroactivity range of the BDD electrode.

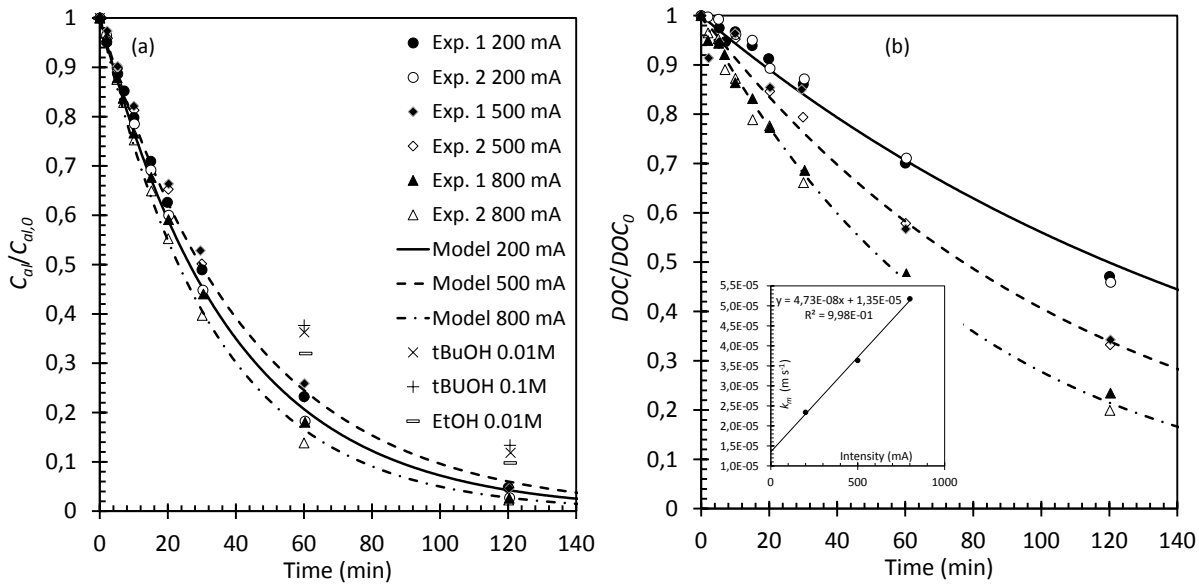

Fig. 5. Time-course profile of $C_{al}/C_{al,0}$ (a) and DOC/DOC_0 (b) by anodic oxidation during anodic oxidation without ozone at different current intensity (pH 5, V_L = 800 mL, $C_{al,0}$ ~ 108 μM, $C_{L,oz,0}$ ~ 0 μM). Circles: duplicate experiments at 200 mA, Diamonds: duplicate experiments at 500 mA, Triangles: duplicate experiments at 800 mA. Cross and rod symbols correspond to experiments at 200 mA with addition of radical scavengers (tBuOH and EtOH). Fig. 5.b inset: Evolution of k_m vs. the current intensity. Straight and dash lines represent the kinetic model (Eq. 10).

Table 2. Values of the apparent first-order reaction rate constants accounting for alachlor and DOC oxidation (k_{app}), corresponding half-life times, values of k_m, $J_{lim,0}$ and $J_{applied}/J_{lim,0}$ during anodic oxidation without ozone at different current intensity (pH 5, V_L = 800 mL, $C_{al,0}$ ~ 108 μM, $C_{L,oz,0}$ ~ 0 μM).

	200 mA	500 mA	800 mA	200 mA with tBuOH
$k_{app,al}$ (s^{-1})	4.37×10^{-4}	3.90×10^{-4}	5.00×10^{-4}	2.8×10^{-4}
$t_{1/2}$ alachlore (min)	26	30	23	42
ARE (C_{al})	4%	5%	4%	4%
$k_{app,DOC}$ (s^{-1})	0.97×10^{-4}	1.50×10^{-4}	2.14×10^{-4}	Not applicable
$t_{1/2}$ DOC (min)	120	77	54	
ARE (DOC)	2%	3%	1%	
$10^5 \times k_m$ (m s^{-1})	2.34	3.64	5.18	
$J_{lim,0}$ (A m^{-2})	18.4	28.7	40.8	
$J_{applied}/J_{lim,0}$	3.3	5.3	5.9	

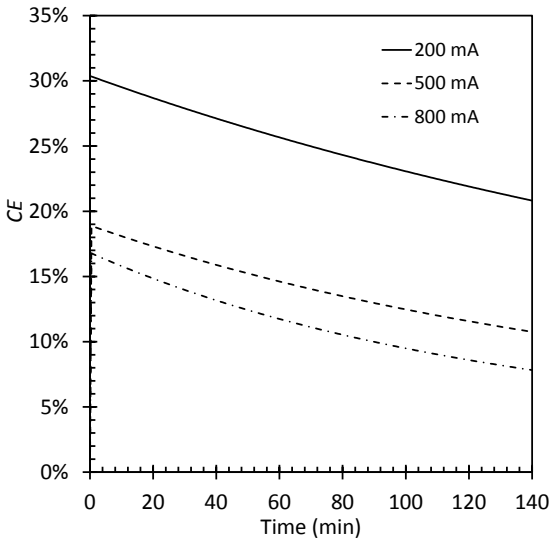

Fig. 6. Evolution of the current efficiency vs. time for different current intensity during alachlor anodic oxidation (pH 5, V_L = 800 mL, $C_{al,0}$ ~ 108 μM, $C_{L,oz,0}$ ~ 0 μM).

3.5. Hybrid ozonation anodic oxidation

The ozone concentration time-course profile for different current intensities using the hybrid process O_3/AO is represented in Fig. 7.a. The ozone consumption rate was significantly enhanced compared to the experiments with no power input (Fig. 4.a), showing that the anodic oxidation process contributes to molecular ozone consumption. This consumption can be attributed to several promotion reactions: the ozone reaction with hydroxyl radicals produced at the anode, which provides the hydroperoxyl radical $HO_2^{\bullet}$, and/or the ozone electroreduction at the cathode which provides an ozonide radical $O_3^{\bullet-}$ [45]. Local higher pH at the cathode vicinity might be also a way of enhancing ozone decomposition through the initiation reaction with HO^-. Nonetheless, a pH of ~ 9 would be necessary to get a reaction rate with HO^- similar to the apparent one.

There was no statistical difference on the ozone consumption rate (Fig. 7.a) depending on the applied current intensity, which is in agreement with the observation already done for alachlor without ozone (Fig. 5.a). The ozone consumption rate was successfully modeled by a first-order reaction law, with an average half-life time of 4.5 min (Table 3), 2.7 times lower than the half-life time found for the reference experiment with the non-polarized electrodes (12 min).

The enhanced ozone depletion might result in an enhanced ROS generation, which was confirmed by a quick drop of the alachlor concentration (Fig. 5.b). A first-order reaction law poorly described the alachlor depletion. The best agreement was obtained with a second-order reaction law ($k_{app} \times C_{al}^2$), which better described the sharp decreasing observed during the first twenty minutes when residual ozone was still present in the solution. The alachlor degradation rate law was not significantly influenced by the current intensity and the corresponding half-life time was around 12 min, which was half the value found without ozone added to the solution (Tables 2 and 3). It shows that the ozone addition can efficiently enhance the alachlor parent molecule degradation rate.

Addition of tBuOH as a radical scavenger allowed to slow down the ozone depletion, but with still a rather fast ozone consumption rate, characterized by a half-life time around 10-11 min, whereas a half-life time of 42 min was found with the non-polarized electrodes in presence of tBuOH. tBuOH efficiently scavenges free $HO^{\bullet}$ radicals in the solution [70]. Without current intensity, the ozone depletion was therefore only due to reactions between molecular ozone and the parent alachlor molecules and its intermediates when tBuOH was present in the solution. The faster ozone consumption rate observed with the hybrid O_3/AO oxidation process in presence of tBuOH in solution confirms that at least one mechanism contributes to molecular ozone consumption at the anode and/or at the cathode. The alachlor consumption rate was also significantly slowed down using a radical scavenger (Table 3 and Fig. 7.b). This confirms that even if molecular ozone was consumed at the anode and/or the cathode, it results in the formation of free hydroxyl radicals that were efficiently scavenged by tBuOH.

In terms of mineralization, assessed through DOC measurement between 0 and 40 min, the results are more difficult to interpret (Fig. 8). The DOC depletion was well described by a first-order reaction law, demonstrating the reaction is still diffusion controlled (Table 3). The mineralization rate at 200 mA is identical between AO alone and the hybrid process AO/O_3. However, the mineralization rate is not significantly different at 500 and 800 mA and is between the rate observed at 500 and 800 mA

without ozone. This behavior might be due to analytical uncertainties and remains unexplained, especially because DOC concentration was only followed during a shorter reaction time of 40 min. Whatever, it shows that the ozone addition poorly influence the mineralization rate. This observation is in agreement with the fact that the ozone dose introduced (around 2 mol of O_3 per mol of alachlor) is far from the theoretical ozone consumption of 38/3 mol_{O_3} mol_{al}^{-1} in case of a total mineralization, according to Eq. 15 :

$$C_{14}H_{20}ClNO_2 + 38/3\ O_3 \rightarrow 14\ CO_2 + 2H^+ + NO_3^- + Cl^- + 9\ H_2O \qquad \text{(Eq. 15)}$$

Consequently, ozone addition could be a potent solution to enhance the degradation of both the alachlor parent molecule and maybe the first aromatic intermediates [68], even if O_3 is quickly consumed in solution (~ 25 min). Nonetheless, low-chain aliphatic acids intermediates must quickly accumulate in solution after a few tens of minutes. These compounds are quite refractory to hydroxyl radicals oxidation as mentioned before (Part 3.4.1), and ozonation as well, and cannot end up fully mineralized by anodic oxidation [71]. They can also reduce the activity of the electrodes due to poisoning effects caused by polymer production on the electrode surface [71]. Thus, in order to increase the time window in which ozone is present in solution, pulse injection of ozone could be a pertinent solution.

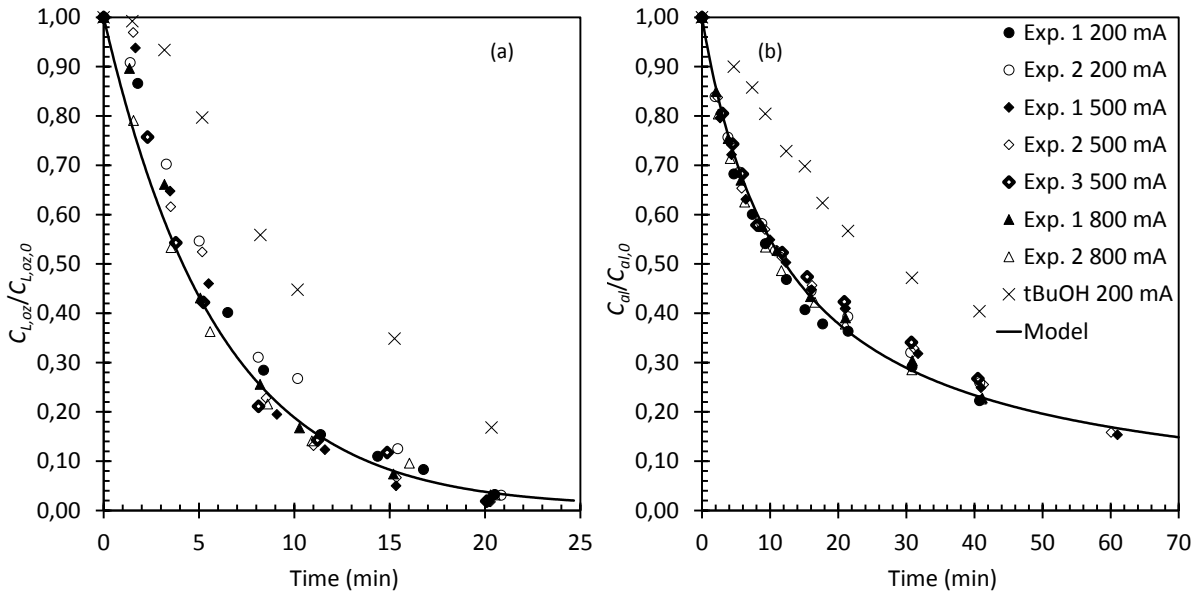

Fig. 7. Time-course profile of $C_{L,oz}/C_{L,oz,0}$ (a) and $C_{al}/C_{al,0}$ (b) by the hybrid process O_3/AO with various current intensity (pH 5, V_L = 800 mL, $C_{al,0}$ ~ 108 μM, $C_{L,oz,0}$ ~ 200-250 μM). Circles: duplicate experiments at 200 mA, Diamond: triplicate experiments at 500 mA, Triangle: duplicate experiments at 800 mA. Cross symbols correspond to one experiment at 200 mA with addition of a radical scavenger (tBuOH at 0.1 M). Models correspond to first-order (ozone) and second-order (alachlor) reaction laws.

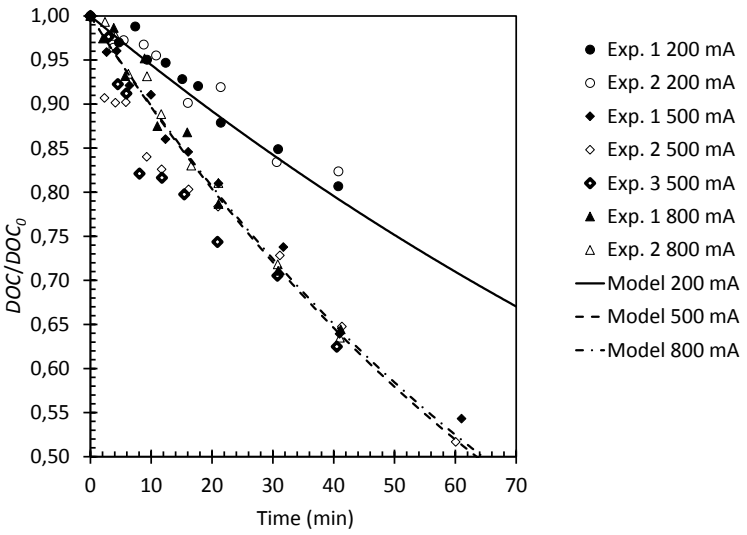

Fig. 8. Time-course profile of DOC/DOC_0 by the hybrid process O_3/AO with various current intensity (pH 5, V_L = 800 mL, $C_{al,0}$ ~ 108 μM, $C_{L,oz,0}$ ~ 200-250 μM). Circles: duplicate experiments at 200 mA, Diamond: triplicate experiments at 500 mA, Triangle: duplicate experiments at 800 mA. Models correspond to a first-order reaction law.

Table 3. Values of the n^{th}-order reaction rate constant accounting for ozone, alachlor and DOC oxidation (k_{app}) and corresponding half-life times by the hybrid process O_3/AO with various current intensity (pH 5, V_L = 800 mL, $C_{al,0}$ ~ 108 μM, $C_{L,oz,0}$ ~ 200-250 μM). For DOC, the half-life time is replaced by the time necessary to degrade 20% ($t_{0.2}$) owing to the fact that the half-life times were higher than the experiment duration.

	200 mA	500 mA	800 mA
First-order $k_{app,oz}$ (s^{-1})		2.59×10^{-3}	
$t_{1/2}$ ozone (min)		4.5	
ARE ($C_{L,oz,0}$)		12%	
n_{al}		2	
2nd-order $k_{app,al}$ (L mol^{-1} s^{-1})		12.7	
$t_{1/2}$ alachlore (min)		12	
ARE (C_{al})		5%	
First-order $k_{app,DOC}$ (s^{-1})	0.95×10^{-4}	1.82×10^{-4}	1.79×10^{-4}
$t_{0.2}$DOC (min)	39	20	21
ARE (DOC)	2%	4%	2%

3.6. Hybrid ozonation anodic oxidation with pulse injections of ozone

Pulse re-injections of dissolved ozone were achieved every 20 min with the hybrid process O_3/AO at 200 mA, leading to:

- a total ozone dose of 34 ppm (6.7 mol of ozone introduced per mol of alachlor) with two re-injections of ozone (1h of exposure to ozone) for a first experiment
- a total ozone dose of 57 ppm (11.1 mol of ozone introduced per mol of alachlor) with 9 re-injections of ozone (2h30 of exposure to ozone) for a second experiment.

The volume of dissolved ozone introduced compensated the volume withdrawn for the samples. The dilution induced by these reinjections were taken into account in the mass-balance to quantify DOC and alachlor concentrations time-profile.

Fig. 9 presents the ozone concentration time-course profile for the first experiment. As expected, O_3 was fully consumed within 20-25 min of reaction time after each injection. The ozone concentration evolution was successfully modeled by a first-order rate law, with kapp = 1.92×10^{-3} s^{-1}, in agreement with the behavior observed with the single ozone injection method (part 3.5).

The prolonged exposure to dissolved ozone led to faster alachlor degradation consumption rate (Fig. 10.a), compared to the experiment with only one dissolved injection at t_0 (Part 3.5). The differences between the pulse ozone injection method and the single ozone injection method only appears after around 30 min, *i.e.* when the dissolved ozone concentration becomes negligible with the single ozone injection method. The alachlor reaction rate was satisfactorily described by a first-order rate law, whereas a second-order rate law was necessary with the single ozone injection method (Part 3.5). Thus, after a reaction time of 1h, with the hybrid process at 200 mA, an alachlor removal efficiency around 94% is reached with the pulse ozone injection method (83% for the single ozone injection method, 79% with only anodic oxidation). It confirms that ozone re-injections can be an

549 effective way to enhance the degradation rate pf the alachlor parent molecule and probably of the
550 first aromatic intermediates, with advantageously low ozone doses involved.

551 However, the prolonged exposure to ozone had only a slight effect on DOC mineralization rate (Table
552 4 and Fig.10 b). In that case, the rate limiting steps should be the reactions of ROS with the low-chain
553 aliphatic acids [68], that are poorly reactive with hydroxyl radicals and molecular ozone [5]. To
554 confirm this assumption, a monitoring of the main by-products formed should be necessary. Other
555 mechanisms such as DET should justify the higher capacity of OA itself to mineralize these
556 compounds. Nonetheless, owing to the fact that these compounds are easily biodegradable, it do not
557 justify to use energy consuming AOPs to achieve a full mineralization of the effluent. More
558 particularly, prolonged exposure to ozone is not necessary anymore after the breakage of the
559 aromatic structures of the parent and intermediates molecules. Furthermore, DOC mineralization by
560 the hybrid process with pulse ozone injection should be assessed with more realistic water matrixes,
561 containing EfOM and having different pH.

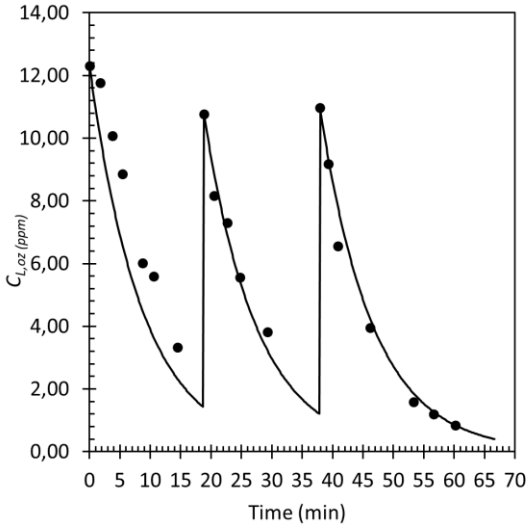

562

563 ***Fig. 9. Time-course profile of $C_{L,oz}$ by the hybrid process with pulse injections of dissolved ozone***
564 ***(pH 5, V_L = 800 mL, $C_{al,0}$ ~ 110 μM, $C_{L,oz,total}$ ~ 709 μM, Intensity = 200 mA). The model corresponds to***
565 ***a first-order reaction law with $k_{app} = 1.92 \times 10^{-3}$ s^{-1}.***

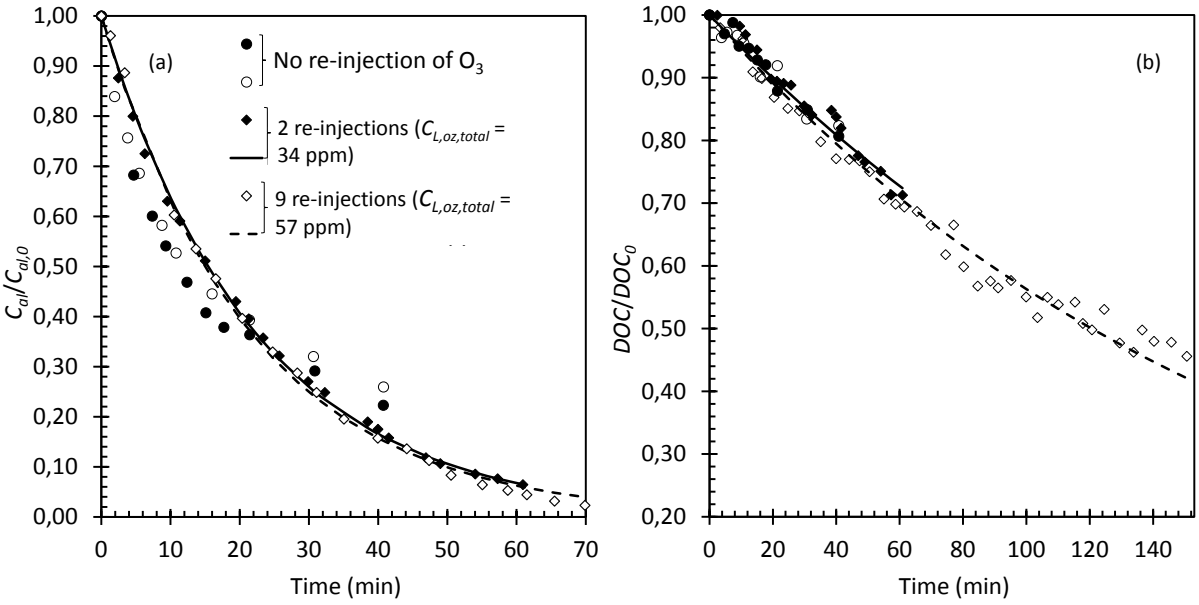

566

567 ***Fig. 10. Time-course profile of $C_{al}/C_{al,0}$ (a) and DOC/DOC_0 (b) by the hybrid process with pulse***
568 ***injections of dissolved ozone (pH 5, V_L = 800 mL, $C_{al,0}$ ~ 110 μM, Intensity = 200 mA). Circles:***
569 ***Experiments with no ozone re-injection; dark diamonds: experiment with two ozone re-injections***
570 ***($C_{L,oz,total}$ ~ 709 μM, 60 min of ozone exposure) and empty diamonds: experiment with nine ozone re-***
571 ***injections ($C_{L,oz,total}$ ~ 1.18 mM, 2h30 of ozone exposure). The models correspond to first-order***
572 ***reaction laws.***

573 ***Table 4. Values of the first-order reaction rate constant accounting for alachlor and DOC***
574 ***oxidation (k_{app}) and corresponding half-life times by the hybrid process O_3/AO with pulse injections***
575 ***of dissolved ozone (pH 5, V_L = 800 mL, $C_{al,0}$ ~ 110 μM, Intensity = 200 mA).***

	2 re-injections	9 re-injections
$C_{L,oz,total}$ (mM)	0.709	1.18
First-order $k_{app,al}$ (s^{-1})	7.49×10^{-4}	7.71×10^{-4}
$t_{1/2}$ alachlore (min)	15	15
ARE (C_{al})	3%	6%
First-order $k_{app,DOC}$ (s^{-1})	8.84×10^{-5}	9.57×10^{-5}
$t_{1/2}$DOC (min)	131	121
ARE (DOC)	2%	3%

576

577

3.7. Diphasic vs monophasic hybrid O_3/AO process; what should be used?

Table 5. Comparison of the monophasic and diphasic hybrid O_3/AO processes.

	Monophasic configuration	Diphasic configuration
Advantages	• Perfect control of the ozone dose and easy optimization of the ozone transfer in a dedicated gaz-liquid contactor • Reactions mainly located in the liquid bulk and at the electrodes surface • Multiple points injection in flow-by or flow-through electrochemical reactors is feasible • Pulse injections or continuous ozone stock solution delivery are both possible in batch electrochemical reactors	• Easier implementation in batch electrochemical reactors • Ozone-enriched bubbles can improve solute mass-transfer in the gas-liquid electrochemical reactor • High ozone doses can be easily implemented
Drawbacks	• High ozone dose hardly achievable • Needs of an additional water resource to prepare the ozone-stock solution (but a fraction of the treated water can be devoted to this) • Needs of an additional gas-liquid contactor	• The control of the ozone dose applied is more difficult owing to the fact that the ozone transfer and ozone reactions steps are interdependent • A significant part or the totality of the ozone transferred can react at the gas-liquid interface • The ozone transfer can be hardly optimized

Parts 3.5 and 3.6 clearly emphasized the pros and cons of the hybrid process O_3/AO. It is noteworthy that an even more enhanced ozone decomposition at the electrode surface might be possible using flow-by or flow-through electrochemical reactors, which are characterized by higher mass-transfer coefficients than conventional agitated electrochemical reactors. These kinds of electrochemical reactors can be easily upgraded for the monophasic configuration of the O_3/AO hybrid process with single or multiple points ozone-stock solution injection. A techno-economical assessment would be pertinent to compare the performances, the energy consumption and the operating and capital expenses of such hybrid processes. Part S.5 in the supplementary material presents some preliminary results regarding these aspects, through the calculation of the Oxygen-equivalent Chemical Oxidation Capacity (OCC), of the Specific Energy Consumption per DOC unit and of the synergy index. Nonetheless, for a full techno-economical assessment, more robust data gathered with realistic industrial wastewaters would be necessary.

593 Table 5 summarizes the main advantages and drawbacks associated to the monophasic and diphasic
594 (use of ozone-enriched gas bubbles) hybrid O_3/AO processes. The superior control of the ozone
595 transfer dose and ozone transfer yield in solution is undoubtedly a salient advantage of the
596 monophasic configuration, allowing to decrease the energy requirement and the operating costs
597 associated to the ozone generation step. Indeed, one of the most challenging issue associated to the
598 use of ozone is the maximization of the ozone transfer yield, which requires a sufficient gas residence
599 time and if possible a low liquid volume (or low liquid flow rate in continuous) owing to the low
600 ozone solubility in water. This constraint can be more easily overcome in a dedicated gas-liquid
601 contactor (agitated vessel, bubble column, static mixer, etc.) than in an electrochemical reactor. In
602 order to maximize the dissolved ozone concentration produced, at a given ozone generator power, a
603 low oxygen flow rate and a large produced ozone concentration should be selected.

604 Another drawback of the diphasic configuration is that ozone transfer directly in the electrochemical
605 reactor might result in a less efficient ROS generation in the liquid bulk. Indeed, depending on the
606 ozone instantaneous ozone demand and on the ozone decomposition rate, a high ozone reaction
607 rate at the gas-liquid interface (fast kinetic regime) is possible [7], which can lead to a poor or even a
608 negligible ozone diffusion in the liquid bulk and at the electrodes surface.

609 The main drawbacks of the monophasic configuration are that supplementary gas-liquid contactor
610 and water resource are necessary for the preparation of the ozone-stock solution. One pertinent
611 solution would be to assess if a fraction of the treated water can be by-passed in the gas-liquid
612 contactor to achieve this operation.

5. Conclusion

This prospective study investigates the efficiency of a hybrid process that combines ozonation and anodic oxidation (AO/O_3) with two boron-doped diamond (BDD) electrodes to treat a model aqueous solution containing 30 ppm of alachlor at pH 5 in a phosphate buffer. An innovative monophasic configuration, in which an ozone-stock solution was injected at t_0 in the batch electrochemical reactor, was proposed in order to avoid the introduction of ozone-enriched gas bubbles.

The results reveal that, even within an acidic water matrix, dissolved ozone injected during the ozonation process was decomposed into hydroxyl radicals allowing to partly degrade alachlor parent molecule but without its mineralization. With the selected water matrix, the hydroxyl radical exposure was particularly low with a R_{ct} value lower than 10^{-10}. The combination of both conventional ozonation and AO processes significantly enhances ozone depletion regardless of the applied current density, resulting in a half-life 2.7 times shorter than the ozonation process alone. This faster ozone decomposition might be related to (i) the ozone oxidation at the anode surface by $OH^{\bullet}$ and/or (ii) to its reduction by the cathode and/or (iii) to its reaction with the electrogenerated hydrogen peroxide, in addition to its decomposition in the bulk. Furthermore, the faster ozone decomposition was concomitant with a higher ROS species generation, which leads to a faster alachlor decomposition, with a half-life twice as low than with AO alone. Thus, this hybrid process is part of the process intensification approach, increasing the operational window for processes use and reducing reaction times.

Regarding alachlor mineralization, increasing the current intensity from 200 mA to 800 mA during the AO process over 120 minutes leads to a rise in alachlor mineralization efficiency from 50 to 80%. However, the introduction of the hybrid process shows a similar mineralization rate as for AO alone. In this case, the limitation could be attributed to the production of refractory biodegradable compounds, such as small aliphatic intermediates (fatty acids), considered to be poorly reactive with hydroxyl radicals and molecular ozone. Moreover, using a pulse injection of ozone every 20 minutes

to extend exposure times and raise the total ozone dose demonstrates only a slight improvement in alachlor mineralization but enhanced the alachlor degradation after the second injection. Thus, the hybrid monophasic AO/O_3 process with a low ozone dose (single ozone injection or a few ozone pulse reinjections) could be sufficient to improve alachlor decomposition into probably more biodegradable compounds that might be more easily removed by a further biological treatment. Nevertheless, further investigation is needed for the identification of the by-products generated. Additionally, using a more realistic water composition containing EfOM, exploring multiple points injection in flow-by or flow-through electrochemical reactors and assessing the feasibility of employing the treated water as a resource for producing stock-ozone solution should be considered.

6. Acknowledgments

The authors gratefully acknowledge the French Ministry of Higher Education, Research and Innovation for providing a PhD grant to Helios Yasmine. The University of Rennes and the ENSCR are also sincerely acknowledged for providing financial supports to this research program. Thierry Pain is thanked for the design and the manufacturing of the glass electrochemical reactor. Etienne Bresteau Rivoal, Océane Turquetil and Catherine Couriol are thanked for their help on this project.

References list

[1] R. Gulde, B. Clerc, M. Rutsch, J. Helbing, E. Salhi, C.S. McArdell, U. von Gunten, Oxidation of 51 micropollutants during drinking water ozonation: Formation of transformation products and their fate during biological post-filtration, Water Res. 207 (2021) 117812. https://doi.org/10.1016/j.watres.2021.117812.

[2] U. Von Gunten, Oxidation processes in water treatment: are we on track?, Environ. Sci. Technol. 52 (2018) 5062–5075.

[3] C. Von Sonntag, U. Von Gunten, Chemistry of ozone in water and wastewater treatment: From basic principles to applications, IWA Publishing, 2012.

[4] U. Von Gunten, Ozonation of drinking water: Part I. Oxidation kinetics and product formation, Water Res. 37 (2003) 1443–1467.

[5] S. Lim, J.L. Shi, U. von Gunten, D.L. McCurry, Ozonation of organic compounds in water and wastewater: A critical review, Water Res. 213 (2022) 118053. https://doi.org/10.1016/j.watres.2022.118053.

[6] D. Gardoni, A. Vailati, R. Canziani, Decay of Ozone in Water: A Review, Ozone Sci. Eng. 34 (2012) 233–242. https://doi.org/10.1080/01919512.2012.686354.

[7] F.J. Beltrán, Ozone reaction kinetics for water and wastewater systems, Lewis Publisher, Boca Raton, 2004.

[8] J. Staehelin, J. Hoigne, Decomposition of ozone in water: rate of initiation by hydroxide ions and hydrogen peroxide, Environ. Sci. Technol. 16 (1982) 676–681.

[9] M.O. Buffle, U. Von Gunten, Phenols and amine induced HO° generation during the initial phase of natural water ozonation, Environ. Sci. Technol. 40 (2006) 3057–3063.

[10] D. Zhi, J. Wang, Y. Zhou, Z. Luo, Y. Sun, Z. Wan, L. Luo, D.C.W. Tsang, D.D. Dionysiou, Development of ozonation and reactive electrochemical membrane coupled process: Enhanced tetracycline mineralization and toxicity reduction, Chem. Eng. J. 383 (2020) 123149. https://doi.org/10.1016/j.cej.2019.123149.

[11] A. Fitch, P. Balderas-Hernandez, J.G. Ibanez, Electrochemical technologies combined with physical, biological, and chemical processes for the treatment of pollutants and wastes: A review, J. Environ. Chem. Eng. 10 (2022) 107810. https://doi.org/10.1016/j.jece.2022.107810.

[12] H. Wang, J. Zhan, L. Gao, G. Yu, S. Komarneni, Y. Wang, Kinetics and mechanism of thiamethoxam abatement by ozonation and ozone-based advanced oxidation processes, J. Hazard. Mater. 390 (2020) 122180. https://doi.org/10.1016/j.jhazmat.2020.122180.

[13] H. Wang, M. Mustafa, G. Yu, M. Östman, Y. Cheng, Y. Wang, M. Tysklind, Oxidation of emerging biocides and antibiotics in wastewater by ozonation and the electro-peroxone process, Chemosphere. 235 (2019) 575–585. https://doi.org/10.1016/j.chemosphere.2019.06.205.

[14] I. Bavasso, D. Montanaro, E. Petrucci, Ozone-based electrochemical advanced oxidation processes, Curr. Opin. Electrochem. 34 (2022) 101017. https://doi.org/10.1016/j.coelec.2022.101017.

[15] J. Zhan, Z. Li, G. Yu, X. Pan, J. Wang, W. Zhu, X. Han, Y. Wang, Enhanced treatment of pharmaceutical wastewater by combining three-dimensional electrochemical process with ozonation to in situ regenerate granular activated carbon particle electrodes, Sep. Purif. Technol. 208 (2019) 12–18. https://doi.org/10.1016/j.seppur.2018.06.030.

[16] M. Rodríguez-Peña, J.A. Barrios Pérez, J. Llanos, C. Sáez, M.A. Rodrigo, C.E. Barrera-Díaz, New insights about the electrochemical production of ozone, Curr. Opin. Electrochem. 27 (2021) 100697. https://doi.org/10.1016/j.coelec.2021.100697.

[17] D. Palomares-Reyna, J.E. Carrera-Crespo, F.S. Sosa-Rodríguez, U.M. García-Pérez, I. Fuentes-Camargo, L. Lartundo-Rojas, J. Vazquez-Arenas, Photo-electrochemical and ozonation process to degrade ciprofloxacin in synthetic municipal wastewater, using C, N-codoped TiO2 with high

visible-light absorption, J. Environ. Chem. Eng. 10 (2022) 107380. https://doi.org/10.1016/j.jece.2022.107380.
[18] B.M. Souza-Chaves, M. Dezotti, C.D. Vecitis, Synergism of ozonation and electrochemical filtration during advanced organic oxidation, J. Hazard. Mater. 382 (2020) 121085. https://doi.org/10.1016/j.jhazmat.2019.121085.
[19] L.A. Bernal-Martínez, C. Barrera-Díaz, C. Solís-Morelos, R. Natividad, Synergy of electrochemical and ozonation processes in industrial wastewater treatment, Chem. Eng. J. 165 (2010) 71–77. https://doi.org/10.1016/j.cej.2010.08.062.
[20] M.A. García-Morales, G. Roa-Morales, C. Barrera-Díaz, B. Bilyeu, M.A. Rodrigo, Synergy of electrochemical oxidation using boron-doped diamond (BDD) electrodes and ozone (O3) in industrial wastewater treatment, Electrochem. Commun. 27 (2013) 34–37. https://doi.org/10.1016/j.elecom.2012.10.028.
[21] S.P. Ghuge, A.K. Saroha, Catalytic ozonation for the treatment of synthetic and industrial effluents - Application of mesoporous materials: A review, J. Environ. Manage. 211 (2018) 83–102. https://doi.org/10.1016/j.jenvman.2018.01.052.
[22] L.M. Da Silva, L.A. De Faria, J.F.C. Boodts, Electrochemical ozone production: influence of the supporting electrolyte on kinetics and current efficiency, Electrochimica Acta. 48 (2003) 699–709. https://doi.org/10.1016/S0013-4686(02)00739-9.
[23] D. Amado-Piña, G. Roa-Morales, C. Barrera-Díaz, P. Balderas-Hernandez, R. Romero, E. Martín Del Campo, R. Natividad, Synergic effect of ozonation and electrochemical methods on oxidation and toxicity reduction: Phenol degradation, Fuel. 198 (2017) 82–90. https://doi.org/10.1016/j.fuel.2016.10.117.
[24] O.M. Cornejo, J.L. Nava, Mineralization of the antibiotic levofloxacin by the electro-peroxone process using a filter-press flow cell with a 3D air-diffusion electrode, Sep. Purif. Technol. 254 (2021) 117661. https://doi.org/10.1016/j.seppur.2020.117661.
[25] O.M. Cornejo, M. Ortiz, Z.G. Aguilar, J.L. Nava, Degradation of Acid Violet 19 textile dye by electro-peroxone in a laboratory flow plant, Chemosphere. 271 (2021) 129804. https://doi.org/10.1016/j.chemosphere.2021.129804.
[26] O.M. Cornejo, J.L. Nava, Incineration of the antibiotic chloramphenicol by electro-peroxone using a smart electrolyzer that produces H2O2 through electrolytic O2, Sep. Purif. Technol. 282 (2022) 120021. https://doi.org/10.1016/j.seppur.2021.120021.
[27] H. Wang, S. Sun, Y. Zhang, S. Chen, P. Liu, B. Liu, An off-line high pH reversed-phase fractionation and nano-liquid chromatography–mass spectrometry method for global proteomic profiling of cell lines, J. Chromatogr. B. 974 (2015) 90–95. https://doi.org/10.1016/j.jchromb.2014.10.031.
[28] A. Da Pozzo, E. Petrucci, C. Merli, Electrogeneration of hydrogen peroxide in seawater and application to disinfection, J. Appl. Electrochem. 38 (2008) 997–1003. https://doi.org/10.1007/s10800-008-9524-4.
[29] X. Li, Y. Wang, S. Yuan, Z. Li, B. Wang, J. Huang, S. Deng, G. Yu, Degradation of the anti-inflammatory drug ibuprofen by electro-peroxone process, Water Res. 63 (2014) 81–93. https://doi.org/10.1016/j.watres.2014.06.009.
[30] I. Bavasso, D. Montanaro, L. Di Palma, E. Petrucci, Electrochemically assisted decomposition of ozone for degradation and mineralization of Diuron, Electrochimica Acta. 331 (2020) 135423. https://doi.org/10.1016/j.electacta.2019.135423.
[31] D. Wu, G. Lu, J. Yao, C. Zhou, F. Liu, J. Liu, Adsorption and catalytic electro-peroxone degradation of fluconazole by magnetic copper ferrite/carbon nanotubes, Chem. Eng. J. 370 (2019) 409–419. https://doi.org/10.1016/j.cej.2019.03.192.
[32] Y. Jiang, H. Zhao, J. Liang, L. Yue, T. Li, Y. Luo, Q. Liu, S. Lu, A.M. Asiri, Z. Gong, X. Sun, Anodic oxidation for the degradation of organic pollutants: Anode materials, operating conditions and mechanisms. A mini review, Electrochem. Commun. 123 (2021) 106912. https://doi.org/10.1016/j.elecom.2020.106912.

[33] C. Trellu, Y. Péchaud, N. Oturan, E. Mousset, D. Huguenot, E.D. Van Hullebusch, G. Esposito, M.A. Oturan, Comparative study on the removal of humic acids from drinking water by anodic oxidation and electro-Fenton processes: Mineralization efficiency and modelling, Appl. Catal. B Environ. 194 (2016) 32–41. https://doi.org/10.1016/j.apcatb.2016.04.039.
[34] B.P. Chaplin, Critical review of electrochemical advanced oxidation processes for water treatment applications, Env. Sci Process. Impacts. 16 (2014) 1182–1203. https://doi.org/10.1039/C3EM00679D.
[35] R. Fu, P.-S. Zhang, Y.-X. Jiang, L. Sun, X.-H. Sun, Wastewater treatment by anodic oxidation in electrochemical advanced oxidation process: Advance in mechanism, direct and indirect oxidation detection methods, Chemosphere. 311 (2023) 136993. https://doi.org/10.1016/j.chemosphere.2022.136993.
[36] C.A. Martínez-Huitle, M. Panizza, Electrochemical oxidation of organic pollutants for wastewater treatment, Curr. Opin. Electrochem. 11 (2018) 62–71. https://doi.org/10.1016/j.coelec.2018.07.010.
[37] S.O. Ganiyu, C.A. Martínez-Huitle, M.A. Oturan, Electrochemical advanced oxidation processes for wastewater treatment: Advances in formation and detection of reactive species and mechanisms, Curr. Opin. Electrochem. 27 (2021) 100678. https://doi.org/10.1016/j.coelec.2020.100678.
[38] E.-M. Buchner, O. Happel, C.K. Schmidt, M. Scheurer, B. Schmutz, M. Kramer, M. Knauer, S. Gartiser, H. Hollert, Approach for analytical characterization and toxicological assessment of ozonation products in drinking water on the example of acesulfame, Water Res. 153 (2019) 357–368. https://doi.org/10.1016/j.watres.2019.01.018.
[39] M. Panizza, G. Cerisola, Direct And Mediated Anodic Oxidation of Organic Pollutants, Chem. Rev. 109 (2009) 6541–6569. https://doi.org/10.1021/cr9001319.
[40] A.R. Rahmani, D. Nematollahi, M.R. Samarghandi, M.T. Samadi, G. Azarian, A combined advanced oxidation process: Electrooxidation-ozonation for antibiotic ciprofloxacin removal from aqueous solution, J. Electroanal. Chem. 808 (2018) 82–89. https://doi.org/10.1016/j.jelechem.2017.11.067.
[41] C.E. Barrera-Díaz, B.A. Frontana-Uribe, M. Rodríguez-Peña, J.C. Gomez-Palma, B. Bilyeu, Integrated advanced oxidation process, ozonation-electrodegradation treatments, for nonylphenol removal in batch and continuous reactor, Catal. Today. 305 (2018) 108–116. https://doi.org/10.1016/j.cattod.2017.09.003.
[42] C. de Leon-Condes, C. Barrera-Díaz, J. Barrios, E. Becerril, H. Reyes-Pérez, A coupled ozonation–electrooxidation treatment for removal of bisphenol A, nonylphenol and triclosan from wastewater sludge, Int. J. Environ. Sci. Technol. 14 (2017) 707–716. https://doi.org/10.1007/s13762-016-1178-x.
[43] M. Faouzi Elahmadi, N. Bensalah, A. Gadri, Treatment of aqueous wastes contaminated with Congo Red dye by electrochemical oxidation and ozonation processes, J. Hazard. Mater. 168 (2009) 1163–1169. https://doi.org/10.1016/j.jhazmat.2009.02.139.
[44] B. Bakheet, C. Qiu, S. Yuan, Y. Wang, G. Yu, S. Deng, J. Huang, B. Wang, Inhibition of polymer formation in electrochemical degradation of p-nitrophenol by combining electrolysis with ozonation, Chem. Eng. J. 252 (2014) 17–21. https://doi.org/10.1016/j.cej.2014.04.103.
[45] C. Qiu, S. Yuan, X. Li, H. Wang, B. Bakheet, S. Komarneni, Y. Wang, Investigation of the synergistic effects for p-nitrophenol mineralization by a combined process of ozonation and electrolysis using a boron-doped diamond anode, J. Hazard. Mater. 280 (2014) 644–653. https://doi.org/10.1016/j.jhazmat.2014.09.001.
[46] M.-O. Buffle, J. Schumacher, S. Meylan, M. Jekel, U. von Gunten, Ozonation and advanced oxidation of wastewater: Effect of O3 dose, pH, DOM and HO•-scavengers on ozone decomposition and HO• generation, Ozone Sci Eng. 28 (2006) 247.
[47] P.-F. Biard, T.T. Dang, J. Bocanegra, A. Couvert, Intensification of the O_3/H_2O_2 advanced oxidation process using a continuous tubular reactor filled with static mixers: Proof of concept, Chem. Eng. J. 344 (2018) 574–582. https://doi.org/10.1016/j.cej.2018.03.112.

[48] S. Ouali, P.-F. Biard, P. Loulergue, R. You, N. Nasrallah, R. Maachi, A. Szymczyk, Water treatment intensification using a monophasic hybrid process coupling nanofiltration and ozone/hydrogen peroxide advanced oxidation, Chem. Eng. J. 437 (2022) 135263. https://doi.org/10.1016/j.cej.2022.135263.
[49] T.T. Dang, P.-F. Biard, A. Couvert, Assessment of a Stirred-Cell Reactor Operated Semicontinuously for the Kinetic Study of Fast Direct Ozonation Reactions by Reactive Absorption, Ind. Eng. Chem. Res. 55 (2016) 8058–8069. https://doi.org/10.1021/acs.iecr.6b02025.
[50] H. Bader, J. Hoigne, Determination of ozone in water by the Indigo method, Water Res. 15 (1981) 1573–1580.
[51] W.Y. He, J.-M. Fontmorin, P. Hapiot, I. Soutrel, D. Floner, F. Fourcade, A. Amrane, F. Geneste, A new bipyridyl cobalt complex for reductive dechlorination of pesticides, Electrochimica Acta. 207 (2016) 313–320. https://doi.org/10.1016/j.electacta.2016.04.170.
[52] I.A. Katsoyiannis, S. Canonica, U. von Gunten, Efficiency and energy requirements for the transformation of organic micropollutants by ozone, O_3/H_2O_2 and UV/H_2O_2, Water Res. 45 (2011) 3811–3822. http://dx.doi.org/10.1016/j.watres.2011.04.038.
[53] A. Abou Dalle, L. Domergue, F. Fourcade, A.A. Assadi, H. Djelal, T. Lendormi, I. Soutrel, S. Taha, A. Amrane, Efficiency of DMSO as hydroxyl radical probe in an Electrochemical Advanced Oxidation Process − Reactive oxygen species monitoring and impact of the current density, Electrochimica Acta. 246 (2017) 1–8. https://doi.org/10.1016/j.electacta.2017.06.024.
[54] J. Ferre-Aracil, S.C. Cardona, J. Navarro-Laboulais, Determination and validation of Henry's Constant for Ozone in Phosphate Buffers using different analytical methodologies, Ozone Sci. Eng. 37 (2015) 106–118.
[55] P.-F. Biard, B. Werghi, I. Soutrel, R. Orhand, A. Couvert, A. Denicourt-Nowicki, A. Roucoux, Efficient catalytic ozonation by ruthenium nanoparticles supported on SiO_2 or TiO_2: Towards the use of a non-woven fiber paper as original support, Chem. Eng. J. 289 (2016) 374–381.
[56] F.J. Beltrán, M. González, F.J. Rivas, B. Acedo, Determination of Kinetic Parameters of Ozone During Oxidations of Alachlor in Water, Water Environ. Res. 72 (2000) 689–697. https://doi.org/10.2175/106143000X138300.
[57] M.S. Elovitz, U. Von Gunten, Hydroxyl radical/ozone ratios during ozonation processes. I. The R_{ct} concept, Ozone Sci. Eng. 21 (1999) 239–260.
[58] P.-F. Biard, T.T. Dang, A. Couvert, Determination by reactive absorption of the rate constant of the ozone reaction with the hydroperoxide anion, Chem. Eng. Res. Des. 127 (2017) 62–71.
[59] T. Mizuno, H. Tsuno, H. Yamada, Development of ozone self-decomposition model for engineering design, Ozone Sci. Eng. 29 (2007) 55–63.
[60] K. Chelkowska, D. Grasso, I. Fábián, G. Gordon, Numerical simulations of aqueous ozone decomposition, (1992).
[61] R.E. Buehler, J. Staehelin, J. Hoigne, Ozone Decomposition in Water Studied by Pulse Radiolysis 1. $HO_2°/O_2^{-}°$ and $HO_3°/O_3^{°-}$ as Intermediates - Correction, J. Phys. Chem. 88 (1984) 5450–5450.
[62] R.E. Buehler, J. Staehelin, J. Hoigne, Ozone decomposition in water studied by pulse radiolysis. 1. Perhydroxyl (HO_2)/hyperoxide ($O_2^{-}°$) and $HO_3°/O_3^{-}°$ as intermediates, J. Phys. Chem. 88 (1984) 2560–2564.
[63] E.L. Yong, Y.-P. Lin, Incorporation of initiation, promotion and inhibition in the R_{ct} concept and its application in determining the initiation and inhibition capacities of natural water in ozonation, Water Res. 46 (2012) 1990–1998.
[64] M. Panizza, P.A. Michaud, G. Cerisola, Ch. Comninellis, Anodic oxidation of 2-naphthol at boron-doped diamond electrodes, J. Electroanal. Chem. 507 (2001) 206–214. https://doi.org/10.1016/S0022-0728(01)00398-9.
[65] M.S.E. Abdo, R.S. Al-Ameeri, Anodic oxidation of a direct dye in an electrochemical reactor, J. Environ. Sci. Health Part Environ. Sci. Eng. 22 (1987) 27–45. https://doi.org/10.1080/10934528709375331.

[66] P.N. Johnson, R.A. Davis, Diffusivity of Ozone in Water, J. Chem. Eng. Data. 41 (1996) 1485–1487. https://doi.org/10.1021/je9602125.
[67] R.H. Perry, D.W. Green, Perry's chemical engineers' handbook, 7th edition, McGraw-Hill, New-York, 1997.
[68] Z. Qiang, C. Liu, B. Dong, Y. Zhang, Degradation mechanism of alachlor during direct ozonation and O3/H2O2 advanced oxidation process, Chemosphere. 78 (2010) 517–526. https://doi.org/10.1016/j.chemosphere.2009.11.037.
[69] G.V. Buxton, C.L. Greenstock, W.P. Helman, A.B. Ross, W. Tsang, Critical review of rate constants for reactions of hydrated electrons, hydrogen atoms and hydroxyl radicals ($OH^{\bullet}/O^{\bullet-}$) in aqueous solution, J. Phys. Chem. Ref. Data. 17 (1988) 513–886.
[70] J. Xie, C. Zhang, T.D. Waite, Hydroxyl radicals in anodic oxidation systems: generation, identification and quantification, Water Res. 217 (2022) 118425. https://doi.org/10.1016/j.watres.2022.118425.
[71] R. Fu, P.-S. Zhang, Y.-X. Jiang, L. Sun, X.-H. Sun, Wastewater treatment by anodic oxidation in electrochemical advanced oxidation process: Advance in mechanism, direct and indirect oxidation detection methods, Chemosphere. 311 (2023) 136993. https://doi.org/10.1016/j.chemosphere.2022.136993.
[72] J.M. Barazesh, C. Prasse, D.L. Sedlak, Electrochemical Transformation of Trace Organic Contaminants in the Presence of Halide and Carbonate Ions, Environ. Sci. Technol. 50 (2016) 10143–10152. https://doi.org/10.1021/acs.est.6b02232.